RSC Advances

PAPER

View Article Online
View Journal | View Issue

Cite this: *RSC Adv.*, 2020, **10**, 31165

Functionalized pyridine in pyclen-based iron(III) complexes: evaluation of fundamental properties†

Magy A. Mekhail, Kristof Pota, Timothy M. Schwartz and Kayla N. Green *

Received 1st July 2020
Accepted 4th August 2020

DOI: 10.1039/d0ra05756h

rsc.li/rsc-advances

The use of tetra-aza pyridinophanes is of increasing interest in the fields of bioinorganic modeling, catalysis, and imaging. However, a full study of how modifications to the pyridyl moiety affect the characteristics of the daughter metal complexes, has not been explored. In this study, six tetra-aza macrocyclic ligands were metalated with Fe(III) and were characterized for the first time. The pyridyl functional groups studied include: 4-hydroxyl (**L1**), 4-H (**L2**), 4-chloro (**L3**), 4-trifluoromethyl (**L4**), 4-nitrile (**L5**), and 4-nitro (**L6**) modified pyridyl on a pyclen base structure. The resulting iron complexes were characterized by X-ray diffraction analysis, cyclic voltammetry, and metal-binding affinities (log β) were determined. Analysis of these results indicate that such functionalizations introduce a handle by which electrochemical properties and thermodynamic stability of daughter complexes with transition metal ions can be tuned, which in turn, could potentially impact the reactivity of these complexes in future studies.

Introduction

Porphyrins, corrins, and chlorins are examples of macrocyclic compounds found in nature with vital roles in many animals (hemoglobin) and vegetation (chlorophyll).[1] The reactions carried out by these systems are highly selective and take place under mild experimental conditions.[1] The prospect of using model compounds to emulate such species in catalysis and medicine has been a driving force for efforts focused on the synthesis and modification of macrocyclic ligands dating back to 1926, with the first total synthesis of etioporphyrin-III and octamethylporphyrin.[2] A large library of nitrogen-containing macrocycles has been developed in response to the increasing interest in the study and use of macrocyclic ligands, a class of which are pyridinophanes, also known as pyridine containing macrocycles.[3–5] The unique attributes of introducing a pyridine moiety into macrocycles was recognized early on. For example, pyclen (1,4,7,10-tetra-aza-2,6-pyridinophane, Fig. 1) has conformational rigidity and decreased basicity compared to cyclen.[6] Therefore, the inclusion of pyridine provides an avenue through which thermodynamic properties and complexation kinetics can be modulated.[3–5,7]

Congeners of pyclen have been widely studied to tune their properties and reactivity.[8] For example, it was observed that 12- and 13-membered cavities cannot accommodate planar coordination compared to 14-membered py-2,3-cyclam, which significantly affects the electrochemical properties of the complex and leads to the stabilization of rather uncommon metal oxidation states.[9,10] Introduction of pendant arms, amine functionalization on the macrocycle, and differing numbers of coordinating atoms are all examples of other modifications that have been studied to tune reactivity of pyridinophanes to achieve changes to geometric rigidity, electrochemical properties, and coordination environments, respectively.[11–16] As a result of these modifications, pyridinophanes have been successfully used as mimics of biological systems,[17] scaffolds for magnetic resonance imaging,[18] and ligands for catalysis.[12,19–21]

The impact of the functionalization of the pyridine moiety, which has not been evaluated in pyridinophanes to date, adds a new method of tuning the reactivity of the ligand and the redox activity of a metal chelated to the pyridinophane. Such modifications are anticipated to control the characteristics and reactivity of daughter metal complexes.[22] However, pyridinophanes (PyN_3) with functionalized pyridine rings have been scarcely reported to date, due to synthetic barriers. Our

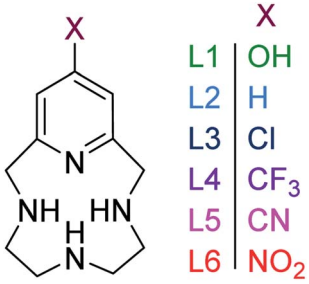

Fig. 1 Pyridinophane macrocycles investigated in this study with different functional groups on the 4-position of the pyridine ring.

Department of Chemistry and Biochemistry, Texas Christian University, 2950 W. Bowie, Fort Worth, TX 76129, USA. E-mail: kayla.green@tcu.edu

† Electronic supplementary information (ESI) available. CCDC 1977733, 1984171–1984175. For ESI and crystallographic data in CIF or other electronic format see DOI: 10.1039/d0ra05756h

Table 1 Selected bond angles (°) and lengths (Å) from single crystal X-ray diffraction analysis of **FeL1**, **FeL2**, **FeL3**, **FeL4**, **FeL5** and **FeL6**

Bond angle (°)/length (Å)	**FeL1** (OH)	**FeL2** (H)	**FeL3** (Cl)	**FeL4** (CF_3)	**FeL5** (CN)	**FeL6** (NO_2)
Cl(1)–Fe–Cl(2)	92.06(3)	98.37(14)	100.084(19)	100.34(2)	92.83(3)	99.95(13)
N(4)–Fe–N(2)	87.23(8)	85.21(4)	84.45(6)	84.52(7)	85.94(14)	84.4(4)
N(3)–Fe–N(1)	148.45(8)	147.08(5)	147.19(6)	147.11(8)	147.32(15)	147.1(4)
Fe–N(1)	2.178(2)	2.178(11)	2.1719(11)	2.1630(14)	2.170(3)	2.169(17)
Fe–N(2)	2.156(2)	2.197(12)	2.2010(15)	2.199(2)	2.157(4)	2.199(2)
Fe–N(3)	2.175(2)	2.158(11)	2.1719(11)	2.1630(14)	2.170(3)	2.169(7)
Fe–N(4)	2.065(2)	2.114(11)	2.1163(15)	2.127(2)	2.105(4)	2.131(2)

group has reported **L1** (Fig. 1), with an –OH in the 4-position of the pyridine ring, as a potential therapeutic for neurodegenerative diseases.[3,23] The former is a daughter molecule to the unsubstituted 12-membered pyridinophane pyclen, henceforth referred to as **L2**.[24,25] Metal complexes derived from **L2** and modifications to the C–C linkers have been extensively explored, as noted above.[8,25–27] The 4-OMe substituted pyridinophane was studied as a precursor to a scaffold used for iron-catalyzed oxidation chemistry.[26] The 4-Br substituted pyridinophane was developed as an intermediate for synthesis of molecules explored for biomedical imaging.[28] Finally, our group has recently synthesized a series of ligands with electron-withdrawing groups (EWG) (**L3–L6**) to diversify pyridinophane chemistry and allow the development of this library.[29]

Here we report the impact of modified pyridine moieties on the iron(III) metal complexes using ligands **L1–L6** (Fig. 1). The functional groups range from electron-donating (ED) (**L1** (OH)) to electron-withdrawing (EW) (**L3** (Cl) < **L4** (CF_3) < **L5** (CN) < **L6** (NO_2)) and will be compared to the unsubstituted **L2** (H). Such modifications are hypothesized to introduce a handle by which electrochemical properties of daughter complexes with transition metal ions can be tuned. The iron(III) complexes were characterized by X-ray diffraction analysis, cyclic voltammetry, and metal-binding affinities.

Results and discussion

Synthesis and X-ray crystallography of iron(III) complexes

Complexation was achieved by mixing equimolar ratios of iron(III) triflate with each ligand (**L1–L6**) in methanol and a minimal amount of water. X-ray quality crystals of **FeL1** (orange), **FeL2**, **FeL3**, **FeL4** and **FeL5** (yellow), and **FeL6** (brown) were obtained through slow evaporation of methanol solutions

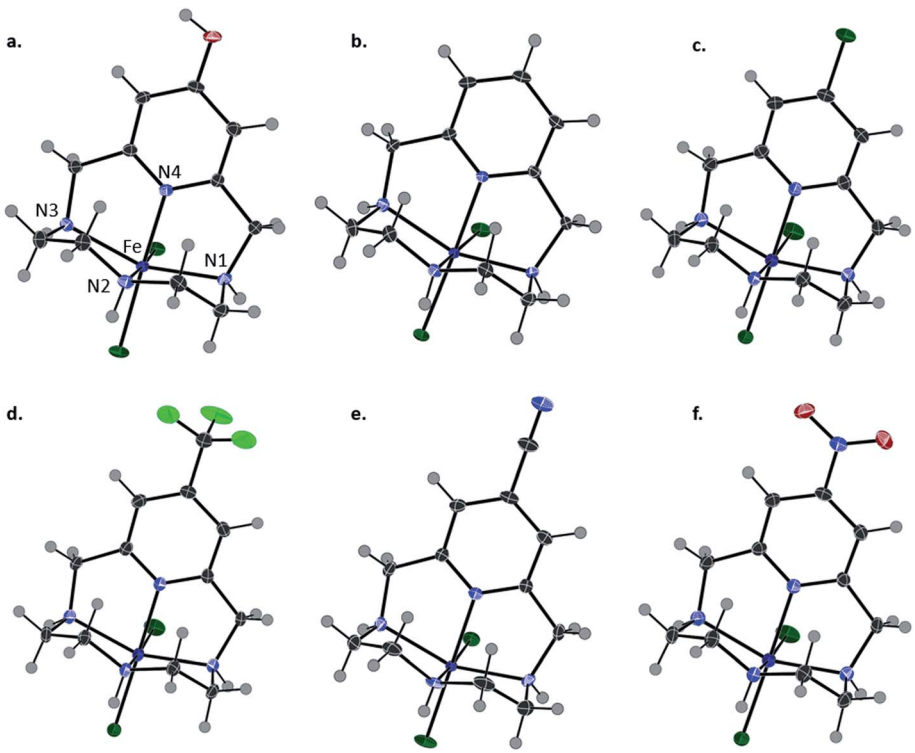

Fig. 2 Solid-state structures of (a) **FeL1** (OH), (b) **FeL2** (H), (c) **FeL3** (Cl), (d) **FeL4** (CF_3), (e) **FeL5** (CN), and (f) **FeL6** (NO_2). Thermal ellipsoids are presented at 50%. Counterions are omitted for clarity.

and used for the analyses described herein. The perchlorate salts of **FeL1** and **FeL2** were previously reported, but triflate salts were produced for consistency in this study.[30] The results from X-ray diffraction analysis show that each complex adopts a six-coordinate, distorted octahedral geometry (N(2)–Fe–N(4) = 84–87°; N(1)–Fe–N(3) = 147–148°) (Table 1 and Fig. 2). The coordination sphere consists of four nitrogen donor atoms from the ligand set: two axial and two equatorial (*cis*). Likewise, two *cis*-coordinated chlorine atoms occupy the remaining equatorial positions around the iron(III) center. A line of symmetry was also observed for **FeL5** and **FeL6** through atoms N(2), Fe(1), and N(4), along with the functional group on the pyridine ring.

The Fe–$N_{pyridine}$ (Fe–N(4)) bond is most likely to be affected by the functionalization of the pyridine ring and was consistently observed to be the smallest of the Fe–N bonds in each complex. Within the series, the shortest Fe–N(4) bond distance (2.065(2)) was observed with **FeL1** (largest EDG character), while the longest (2.131(2)) with **FeL6** (largest EWG character). Compared to **FeL1** and **FeL2**, the more electron withdrawing groups weaken the Fe–$N_{pyridine}$ bond as a result of the decreased localized electron density on the pyridine nitrogen. These results reveal that modifications to the pyridine moiety of the ligand provide subtle changes to the geometry of the complex.

Formation constants

Potentiometric titrations were used to identify correlations between functionalization of the pyridine ring in **5L1–L6** and stability constants (log β) with iron(II) (Tables 2 and S1†). The formation of $Fe(OH)_3$(s) and Fe_2O_3(s) at lower pH values precludes potentiometric titrations in the presence of Fe(III). Therefore, the stability of the Fe(III) species of **L1–L5** was calculated using eqn (1).[31] The binding affinity towards both iron(II) and iron(III) was observed to generally decrease with increased EW character. **L1** (ED) was expected to have a larger stability constant in comparison to **L2**, however the observed data reveals otherwise. As previously observed, this ligand is observed in both enol and keto forms in solution (the ratio between the two is unknown).[6]

The presence of the keto form lowers the formation constant of the iron complex because the non-bonding electron pair from the pyridine N-atom, which would be donated to the metal center, is incorporated as part of the delocalized seven-center eight-electron system. To further support this, the thermodynamic stability with iron(II) decreased as the EW character of the pyridine substitution increased, with the exception of **L4** (Table 2). The observed preference of the electron donating ligand with ferric iron and the electron withdrawing ligands with ferrous iron is perhaps the most obvious evidence that functionalizing the pyridine ring can affect the complexes as a whole. Specifically, the iron(III) complexes derived from **L1** and **L2** were more thermodynamically favorable, compared to the iron(II) congeners. In contrast, larger stability constants were observed between ligands containing EWGs (**L3–L5**) with iron(II) as result of the ligands being electron deficient and, therefore, favoring the lower valent iron cation. Poor solubility of **L6** (NO_2) precluded potentiometric studies. Preliminary results of equilibrium studies of **L4** with other metals reveal the same complexation trends between the divalent and trivalent iron and are the focus of an ongoing study.

Table 2 Formation constants (log β) of the ML species formed, Fe(II)/(III)

	$\log \beta_{red}$	$\log \beta_{ox}$
Complex	Fe(II)[a]	Fe(III)[b]
[Fe(**L1**)]	14.18(5)	14.57
[Fe(**L2**)]	14.46(7)	14.70
[Fe(**L3**)]	12.41(2)	12.02
[Fe(**L4**)]	14.12(4)	13.92
[Fe(**L5**)]	12.30(2)	11.44

[a] I = 0.15 M NaCl and T = 25.0 °C. [b] Derived from eqn (1) (ref. 31) and $(Fe^{2+})_{aq}$, $E^{\circ\prime}Fe^{III}/Fe^{II} = -0.439$ *vs.* $[Fe(CN)_6]^{3-}/[Fe(CN)_6]^{4-}$.

$$\Delta E_{1/2} = E_{1/2,\ \text{complex}} - E_{1/2,\ Fe_{aq}} = -0.59 \log \frac{\beta_{ox}}{\beta_{red}} \quad (1)$$

Electrochemistry

Cyclic voltammetry was used to further evaluate the impact of pyridine substitution on the electrochemical behavior of **FeL1–FeL6.** The cyclic voltammograms show that the iron(III/II) redox couple ranges between −470 mV and −360 mV for the series (Fig. 3). The results indicate that the observed iron(III/II) redox processes are quasi-reversible at 100 mV s^{-1} and diffusion controlled (Table 3), which is consistent with similar complexes in literature.[20,30,32] The **FeL1** ($E_{1/2}$ = −462 mV) complex has the most negative half-cell potential followed by **FeL2** ($E_{1/2}$ = −453 mV). The potentials of the remaining complexes are more positive (favoring reduction) than **FeL1** and **FeL2**, consistent with the pyridine functionalizations, and the most positive value observed with **FeL6** ($E_{1/2}$ = −372 mV). The trend observed is an indication that functionalization of

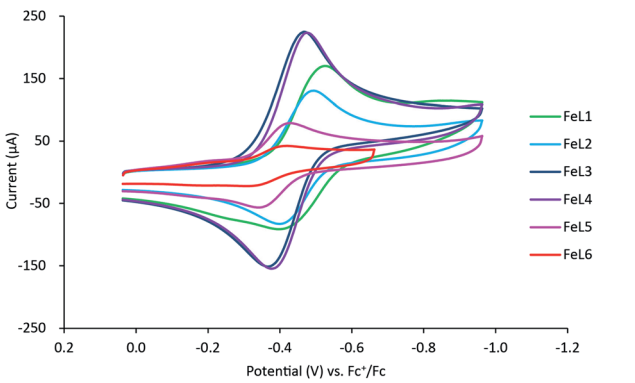

Fig. 3 Cyclic voltammogram overlay of the iron(III/II) redox couple of **FeL1–FeL6** in DMF (3–4 mM) containing $[Bu_4N][BF_4]$ (100 mM) as the supporting electrolyte at a scan rate of 100 mV s^{-1}. The potential values presented here have been normalized to the half-wave potential of the Fc^+/Fc redox couple ($E_{1/2}$ = 0.00 V).

Table 3 The oxidation (E_{Pa}) and reduction (E_{Pc}) potentials (mV), ΔE (mV), and $E_{1/2}$ (mV) for **FeL1–FeL6**

Complexes	E_{Pa} (mV)	E_{Pc} (mV)	ΔE (mV)	$E_{1/2}$ (mV)
FeL1 (OH)	−398	−526	128	−462
FeL2 (H)	−404	−502	98	−453
FeL3 (Cl)	−365	−466	95	−416
FeL4 (CF_3)	−377	−476	99	−427
FeL5 (CN)	−347	−432	85	−388
FeL6 (NO_2)	−330	−414	84	−372

the pyridine ring on the ligand can tune the electrochemical properties of the metal and potentially control reactivity. It is also important to point out that the trend observed with the electrochemical behavior of the iron complexes paralleled the thermodynamic stability determined for the metal complexes. The **FeL4** complex was the exception to the trend observed with both the potentiometric and the electrochemical studies, suggesting there are more factors in play than simply the Hammett parameters derived from substituted benzoic acids.[33] Interestingly, DFT analysis with a range of basis sets and functionals, including B3LYP,[34,35] B3PW91,[35,36] aug-cc-pvdz,[37–39] aug-cc-pvtz,[37–39] lanL2DZ,[40] 6-31++g(d,p),[41–43] 6-31++g(d′,p′),[44] and 6-311++g(d,p),[41,45] was not able to model the solid-state structures or other properties observed. This suggests that more is at play than simple changes to electronics. Such analysis is ongoing.

Additional oxidation (∼−1.5 mV) and reduction (−1.8 to −0.8 mV) events were also observed within the full experimental window of solutions containing **FeL1–FeL6**, which were hypothesized to be ligand-based. Therefore, cyclic voltammetry was conducted for ligands **L1–L6** as well. The redox potentials observed are known to be a result of the pyridine ring.[46] In these studies, reduction events were observed, in addition to the positive ligand-based oxidation reported previously with **L1** and **L2** (Fig. 4).[30,47] Similar trends to the iron(III) complexes were observed for the reduction events in the ligands, where the more EWG character to the pyridine ring correlated to more positive reduction waves. It should be noted that the reduction wave of **L6** (E_{pc} = −783 mV) is significantly more positive compared to the other ligands (Table S14†), almost overlapping with the redox window of iron complexes themselves. Such activity is unique and potentially worthwhile to explore in possible further applications.

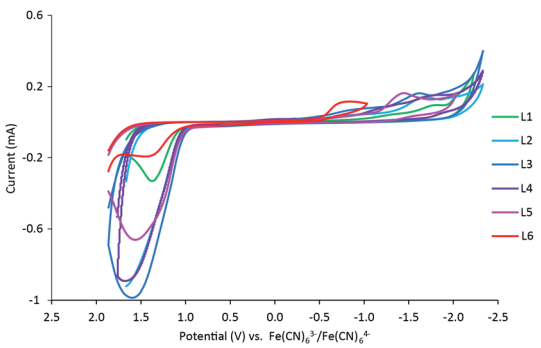

Fig. 4 Cyclic voltammograms obtained for ligands **L1–L6** in 3 mL of 0.1 M $NaCl_{(aq)}$ solution at a scan rate of 100 mV s^{-1} normalized to $[Fe(CN)_6]^{3-}/[Fe(CN)_6]^{4-}$ ($E_{1/2}$ = 0.00 V).

Experimental

General methods

Elemental analysis was performed by Canadian Microanalytical Service Ltd. **L1–L6** were synthesized using previously published procedures and isolated as water soluble trihydrochloride salts.[3,23,29]

Potentiometric methods

The concentration of each ligand, as well as stability constants of the iron(II) complexes, were determined *via* pH-potentiometric titrations. A Metrohm 888 Titrando equipped with a Metrohm 6.0234.100 combined electrode was used to measure the pH in the titration experiments. For the calibration of the electrode, KH-phthalate (pH 4.008) and borax (pH 9.177) buffers were used.[48,49] The calculation of $[H^+]$ from the measured pH values was performed with the use of the method proposed by Irving *et al.* by titrating a 0.02 M HCl solution with a standardized NaOH solution (0.2 M).[50] The differences between the measured and calculated pH values were used to obtain the $[H^+]$ concentrations from the pH-data collected in the titrations. The ion product of water was determined from the same experiment in the pH range 11.40–12.00. The ionic strength in the titrated and thermostat controlled (at 25 °C) samples of 6.00 mL was kept constant and set to 0.15 M NaCl. The samples were stirred by a magnetic stirbar and kept under inert gas atmosphere (N_2) to avoid the effect of CO_2. The protonation constants of the ligands were obtained from previously reported data.[29] The stability constants of the metal complexes were determined using the direct pH-potentiometric method by titrating samples with 1 : 1 metal-to-ligand ratios (the number of data pairs were between 100–250), allowing 1 min for sample equilibration to occur. The protonation and stability constants ($(\log \beta) = [ML]/([M][L])$) were calculated from the titration data with the PSEQUAD program.[51]

Synthesis of iron complexes

$[Fe^{III}L1(Cl)_2]Cl$. $Fe(CF_3SO_3)_3$ (300 mg, 0.905 mmol) was dissolved in 6 mL of methanol and added dropwise to **L1** (448 mg, 1.35 mmol) dissolved in a minimal volume of water. The reaction was allowed to stir overnight. A fine precipitate was removed by filtration through a 0.2 μm nylon filter and the yellow solution was transferred to a test tube for slow evaporation at room temperature. The resulting orange, X-ray quality crystals were isolated *via* filtration and washed with a small amount of cold methanol. Yield: 36% (242 mg, 0.486 mmol). (CCDC#: 1984171).†

$[Fe^{III}L2–6(Cl)_2]CF_3SO_3$. $[Fe^{III}L2–6(Cl)_2]CF_3SO_3$ were produced in an identical manner using 100–250 mg of ligand in each reaction.

$[Fe^{III}L2(Cl)_2]CF_3SO_3$. Orange crystals. Yield: 78% (164 mg, 0.340 mmol). *Elemental analysis*: calc. (found) for $C_{12}H_{18}Cl_2F_3FeN_4O_3S$: C, 29.59 (29.90); H, 3.69 (3.76); N, 11.31 (11.62). (CCDC#: 1977733).†

$[Fe^{III}L3(Cl)_2]CF_3SO_3$. Orange crystals. Yield: 44% (140 mg, 0.271 mmol). *Elemental analysis*: calc. (found) for $C_{12}H_{17}Cl_3F_3FeN_4O_3S$: C, 27.90 (27.60); H, 3.32 (3.09); N, 10.81 (10.44). (CCDC#: 1984172).†

$[Fe^{III}L4(Cl)_2]CF_3SO_3$. Yellow crystals. Yield: 38% (55 mg, 0.101 mmol). *Elemental analysis*: calc. (found) for $C_{13}H_{17}Cl_2F_6FeN_4O_3S$: C, 28.38 (28.40); H, 3.12 (3.02); N, 10.19 (10.09). (CCDC#: 1984173).†

$[Fe^{III}L5(Cl)_2]CF_3SO_3$. Yellow crystals. Yield: 59% (126 mg, 0.232 mmol). *Elemental analysis*: calc. (found) for $C_{14}H_{21}Cl_2F_3FeN_5O_4S$: C, 32.33(32.15); H, 4.65(4.90); N, 10.77(10.67). (CCDC#: 1984174).†

$[Fe^{III}L6(Cl)_2]CF_3SO_3$. Brown crystals. Yield: 39% (85 mg, 0.161 mmol). *Elemental analysis*: calc. (found) for $C_{14}H_{21}Cl_2F_3FeN_5O_4S$: C, 32.42(32.62); H, 4.57 (4.39); N, 14.70 (14.52). (CCDC#: 1984175).†

X-ray crystallography

Crystal diffraction data were collected at 100 K on a Bruker D8 Quest Diffractometer. Data collection, frame integration, data reduction (multi-scan), and structure determination were carried out using APEX2 software.[52] Structural refinements were performed with XSHELL (v 6.3.1), by the full-matrix least-squares method.[53] All non-hydrogen atoms were refined using anisotropic thermal parameters, while the hydrogen atoms were treated as mixed. The ORTEP molecular plots (50%) were produced using APEX2 (Version 2014.9-0).

Electrochemistry

Cyclic voltammetry experiments for the Fe(III) complexes (**FeL1–FeL6**) used 3–4 mM complex and 100 mM $[Bu_4N][BF_4]$ as the supporting electrolyte in DMF. The electrochemical cell was composed of a working glassy carbon electrode, a Pt auxiliary electrode, and a silver wire as the reference electrode. The potential values presented here have been normalized to the half-wave potential of the $Fc^+/Fc = 0.00$ mV. Cyclic voltammetry experiments for ligands **L1–L6** used 3–4 mM of ligand and 100 mM NaCl as the supporting electrolyte in water. The electrochemical cell was composed of a working glassy carbon electrode, a Pt auxiliary electrode, and Ag/AgCl as the reference electrode. The potential values presented here have been normalized to the half-wave potential of the $[Fe(CN)_6]^{3-}/[Fe(CN)_6]^{4-} = 0.00$ mV.

Conclusions

Through this study, a library of 4-substituted pyridinophanes, ranging from electron donating to electron withdrawing, was metalated with iron(III), studied using single crystal X-ray diffraction, electrochemistry, and potentiometric titrations to study the impact of 4-substitution of the pyridine ring on the iron complex. Single crystal X-ray diffraction revealed that the substitution on the pyridine play only a small role in impacting coordination geometry. Cyclic voltammograms revealed that reduction is favored (more positive potentials) in case of ligands with more EW character. The binding stability constants supported the electrochemistry results in revealing that the ligands with EWGs favored Fe(II) over Fe(III). The effect of the substitution observed in the conducted studies points towards a new method of tuning the properties and potentially the reactivity of the iron complex.

Conflicts of interest

There are no conflicts to declare.

Acknowledgements

This work was funded by the National Institutes of Health (R15GM123463). The authors are also grateful for generous financial support from TCU Andrews Institute of Mathematics & Science Education and Cambridge Isotope Laboratories. The authors acknowledge the TCU High-Performance Computing Center for providing HPC resources.

Notes and references

1 E. C. Constable, *Coordination Chemistry of Macrocyclic Compounds*, Oxford University Press, 1999.
2 J. K. H. Fischer, *Justus Liebigs Ann. Chem.*, 1926, **448**, 178–193.
3 K. M. Lincoln, M. E. Offutt, T. D. Hayden, R. E. Saunders and K. N. Green, *Inorg. Chem.*, 2014, **53**, 1406–1416.
4 F. Dioury, S. Sambou, E. Guene, M. Sabatou, C. Ferroud, A. Guy and M. Port, *Tetrahedron*, 2007, **63**, 204–214.
5 R. M. Nunes, R. Delgado, M. F. Cabral, J. Costa, P. Brandao, V. Felix and B. J. Goodfellow, *Dalton Trans.*, 2007, 4536–4545, DOI: 10.1039/b710122h.
6 K. N. Green, K. Pota, G. Tircso, R. A. Gogolak, O. Kinsinger, C. Davda, K. Blain, S. M. Brewer, P. Gonzalez, H. M. Johnston and G. Akkaraju, *Dalton Trans.*, 2019, **48**, 12430–12439.
7 K. P. Guerra, R. Delgado, M. G. B. Drew and V. Felix, *Dalton Trans.*, 2006, 4124–4133, DOI: 10.1039/b603484e.
8 S. Xu, L. Bucinsky, M. Breza, J. Krzystek, C. H. Chen, M. Pink, J. Telser and J. M. Smith, *Inorg. Chem.*, 2017, **56**, 14315–14325.
9 M. Rezaeivala and H. Keypour, *Coord. Chem. Rev.*, 2014, **280**, 203–253.
10 A. M. Herrera, G. V. Kalayda, J. S. Disch, R. P. Wikstrom, I. V. Korendovych, R. J. Staples, C. F. Campana, A. Y. Nazarenko, T. E. Haas and E. V. Rybak-Akimova, *Dalton Trans.*, 2003, 4482–4492, DOI: 10.1039/b308557k.
11 B. Verdejo, A. Ferrer, S. Blasco, C. E. Castillo, J. Gonzalez, J. Latorre, M. A. Manez, M. Garcia Basallote, C. Soriano and E. Garcia-Espana, *Inorg. Chem.*, 2007, **46**, 5707–5719.
12 S. Taktak, W. H. Ye, A. M. Herrera and E. V. Rybak-Akimova, *Inorg. Chem.*, 2007, **46**, 2929–2942.
13 W. H. Ye, R. J. Staples and E. V. Rybak-Akimova, *J. Inorg. Biochem.*, 2012, **115**, 1–12.

14 W. H. Ye, D. M. Ho, S. Friedle, T. D. Palluccio and E. V. Rybak-Akimova, *Inorg. Chem.*, 2012, **51**, 5006–5021.
15 J. Serrano-Plana, W. N. Oloo, L. Acosta-Rueda, K. K. Meier, B. Verdejo, E. Garcia-Espana, M. G. Basallote, E. Munck, L. Que, A. Company and M. Costas, *J. Am. Chem. Soc.*, 2015, **137**, 15833–15842.
16 J. R. Khusnutdinova, J. Luo, N. P. Rath and L. M. Mirica, *Inorg. Chem.*, 2013, **52**, 3920–3932.
17 S. G. Rzuczek, D. S. Pilch, A. Liu, L. Liu, E. J. LaVoie and J. E. Rice, *J. Med. Chem.*, 2010, **53**, 3632–3644.
18 B. Drahos, J. Kotek, I. Cisarova, P. Hermann, L. Helm, I. Lukes and E. Toth, *Inorg. Chem.*, 2011, **50**, 12785–12801.
19 G. Tseberlidis, D. Intrieri and A. Caselli, *Eur. J. Inorg. Chem.*, 2017, 3589–3603, DOI: 10.1002/ejic.201700633.
20 S. M. Brewer, K. R. Wilson, D. G. Jones, E. W. Reinheimer, S. J. Archibald, T. J. Prior, M. A. Ayala, A. L. Foster, T. J. Hubin and K. N. Green, *Inorg. Chem.*, 2018, **57**, 8890–8902.
21 J. Wen, S. Qin, L. F. Ma, L. A. Dong, J. Zhang, S. S. Liu, Y. S. Duan, S. Y. Chen, C. W. Hu and X. Q. Yu, *Org. Lett.*, 2010, **12**, 2694–2697.
22 L. Chiang, K. Herasymchuk, F. Thomas and T. Storr, *Inorg. Chem.*, 2015, **54**, 5970–5980.
23 K. M. Lincoln, P. Gonzalez, T. E. Richardson, D. A. Julovich, R. Saunders, J. W. Simpkins and K. N. Green, *Chem. Commun.*, 2013, **49**, 2712–2714.
24 H. Stetter, W. Frank and R. Mertens, *Tetrahedron*, 1981, **37**, 767–772.
25 J. Costa and R. Delgado, *Inorg. Chem.*, 1993, **32**, 5257–5265.
26 R. X. Fan, J. Serrano-Plana, W. N. Oloo, A. Draksharapu, E. Delgado-Pinar, A. Company, V. Martin-Diaconescu, M. Borrell, J. Lloret-Fillol, E. Garcia-Espana, Y. S. Guo, E. L. Bominaar, L. Que, M. Costas and E. Munck, *J. Am. Chem. Soc.*, 2018, **140**, 3916–3928.
27 G. P. Shkil and R. S. Sagitullin, *Khim. Geterotsikl.*, 1998, 579–602.
28 S. Aime, M. Botta, L. Frullano, S. G. Crich, G. B. Giovenzana, R. Pagliarin, G. Palmisano and M. Sisti, *Chem.–Eur. J.*, 1999, **5**, 1253–1260.
29 A. Yepremyan, M. A. Mekhail, B. P. Niebuhr, K. Pota, N. Sadagopan, T. M. Schwartz and K. N. Green, *J. Org. Chem.*, 2020, **85**, 4988–4998.
30 S. M. Brewer, P. M. Palacios, H. M. Johnston, B. S. Pierce and K. N. Green, *Inorg. Chim. Acta*, 2018, **478**, 139–147.
31 M. Botta, M. Ravera, A. Barge, M. Bottaro and D. Osella, *Dalton Trans.*, 2003, 1628–1633, DOI: 10.1039/b211533f.
32 N. Elgrishi, K. J. Rountree, B. D. McCarthy, E. S. Rountree, T. T. Eisenhart and J. L. Dempsey, *J. Chem. Educ.*, 2018, **95**, 197–206.
33 C. Hansch, A. Leo and R. W. Taft, *Chem. Rev.*, 1991, **91**, 165–195.
34 P. J. Stephens, F. J. Devlin, C. F. Chabalowski and M. J. Frisch, *J. Phys. Chem.*, 1994, **98**, 11623–11627.
35 A. D. Becke, *J. Chem. Phys.*, 1993, **98**, 5648–5652.
36 A. D. Becke, *Phys. Rev. A: At., Mol., Opt. Phys.*, 1988, **38**, 3098–3100.
37 T. H. Dunning, *J. Chem. Phys.*, 1989, **90**, 1007–1023.
38 N. B. Balabanov and K. A. Peterson, *J. Chem. Phys.*, 2005, **123**, 064107.
39 R. A. Kendall, T. H. Dunning and R. J. Harrison, *J. Chem. Phys.*, 1992, **96**, 6796–6806.
40 P. J. Hay and W. R. Wadt, *J. Chem. Phys.*, 1985, **82**, 299–310.
41 T. Clark, J. Chandrasekhar, G. W. Spitznagel and P. V. R. Schleyer, *J. Comput. Chem.*, 1983, **4**, 294–301.
42 P. C. Hariharan and J. A. Pople, *Theor. Chim. Acta*, 1973, **28**, 213–222.
43 W. J. Hehre, R. Ditchfield and J. A. Pople, *J. Chem. Phys.*, 1972, **56**, 2257–2261.
44 G. A. Petersson and M. A. Al-Laham, *J. Chem. Phys.*, 1991, **94**, 6081–6090.
45 R. Krishnan, J. S. Binkley, R. Seeger and J. A. Pople, *J. Chem. Phys.*, 1980, **72**, 650–654.
46 R. A. Lewis, K. C. MacLeod, B. Q. Mercado and P. L. Holland, *Chem. Commun.*, 2014, **50**, 11114–11117.
47 P. Murray, L. Jack, E. J. L. McInnes and L. J. Yellowlees, *Dalton Trans.*, 2010, **39**, 4179–4185.
48 G. G. Manov, N. J. Delollis, P. W. Lindvall and S. F. Acree, *J. Res. Natl. Bur. Stand.*, 1946, **36**, 543–558.
49 G. G. Manov, N. J. Delollis and S. F. Acree, *J. Res. Natl. Bur. Stand.*, 1945, **34**, 115–127.
50 H. M. Irving, M. G. Miles and L. D. Pettit, *Anal. Chim. Acta*, 1967, **38**, 475–488.
51 D. Domyati, S. L. Hope, R. Latifi, M. D. Hearns and L. Tahsini, *Inorg. Chem.*, 2016, **55**, 11685–11693.
52 Bruker Advanced X-ray Solutions, *APEX2, Version 2014.9-0*, Bruker AXS Inc., Madison, WI, 2007.
53 Bruker Advanced X-ray Solutions, *SADABS*, Bruker AXS Inc., Madison, WI, 2001.

